Plasma Sci. Technol. **25** (2023) 045506 (11pp) https://doi.org/10.1088/2058-6272/aca13f

# Experimental study of a neutralizer-free gridded ion thruster using radio-frequency self-bias effect

**Zhi YANG** (杨智)[1], **Honghui GUO** (郭宏辉)[1], **Jinwei BAI** (白进纬)[2], **Yang LI** (李阳)[1], **Yong CAO** (曹勇)[1,*] **and Yu ZHU** (朱雨)[3,*]

[1] School of Mechanical Engineering and Automation, Harbin Institute of Technology (Shenzhen), Shenzhen 518055, People's Republic of China
[2] School of Science, Harbin Institute of Technology (Shenzhen), Shenzhen 518055, People's Republic of China
[3] Shenzhen Ruoyu Technology Co. Ltd, Shenzhen 518116, People's Republic of China

E-mail: yongc@hit.edu.cn and 21417772@qq.com

Received 4 August 2022, revised 3 November 2022
Accepted for publication 8 November 2022
Published 8 February 2023

**Abstract**

An experimental study on the quasi-neutral beam extracted by a neutralizer-free gridded ion thruster prototype was presented. The prototype was designed using an inductively coupled plasma source terminated by a double-grid accelerator. The beam characteristics were compared when the accelerator was radio-frequency (RF) biased and direct-current (DC) biased. An RF power supply was applied to the screen grid via a blocking capacitor for the RF acceleration, and a DC power supply was directly connected to the screen grid for the DC acceleration. Argon was used as the propellant gas. Furthermore, the characteristics of the plasma beam, such as the floating potential, the spatial distribution of ion flux, and the ion energy distribution function (IEDF) were measured by a four-grid retarding field energy analyzer. The floating potential results showed that the beam space charge is compensated in the case of RF acceleration without a neutralizer, which is similar to the case of classical DC acceleration with a neutralizer. The ion flux of RF acceleration is 1.17 times higher than that of DC acceleration under the same DC component voltage between the double-grid. Moreover, there are significant differences in the beam IEDFs for RF and DC acceleration. The IEDF of RF acceleration has a widened and multi-peaked profile, and the main peak moves toward the high-energy region with increasing the DC self-bias voltage. In addition, by comparing the IEDFs with RF acceleration frequencies of 3.9 and 7.8 MHz, it is found that the IEDF has a more centered main peak and a narrower energy spread at a higher frequency.

Keywords: gridded ion thruster, neutralizer-free, RF acceleration, plasma beam

(Some figures may appear in colour only in the online journal)

## 1. Introduction

Electric propulsion (EP) technology, which uses high-speed plasma jets to obtain reverse thrust, has been applied in space maneuvers for flying satellites or spacecraft [1–3]. Ion and Hall thrusters have emerged as the typical representatives [1, 4, 5]. The positive ion beam extracted from the thrusters needs to be compensated by electrons which are emitted from the neutralizer to prevent the thrusters from failing [1, 6]. Although many types of advanced neutralizers have been developed, there are still some urgent problems in response time, material corrosion, and current control [6–9]. The life of the EP system is usually determined by the neutralizer. In addition, the external neutralizer will bring some potential problems, such as communication interference and solar array corrosion [1].

* Authors to whom any correspondence should be addressed.

Many novel neutralizer-free EP concepts have been proposed to eliminate the negative effects of neutralizers, such as pulsed plasma thruster, helicon wave plasma thruster, magnetoplasmadynamic thruster, and micro-cathode vacuum arc thruster [6, 10–16]. PEGASES II is one of the neutralizer-free grid thrusters whose quasi-neutral beam is obtained by alternately extracting positive and negative ions from the plasma source [6, 17]. In recent years, the radio-frequency (RF)-biased grid technology has been applied in gridded ion thruster (GIT) to extract electrons and ions from the same plasma source quasi-simultaneously, which uses RF self-bias effect [18–21]. In this concept, the screen grid is connected to the RF power supply via a blocking capacitor, and the acceleration grid is grounded. This acceleration technology is called the RF acceleration in this paper, corresponding to the direct-current (DC) acceleration in classical GIT. In RF acceleration, ions are continuously accelerated within the grids while electrons are extracted periodically when the sheath collapses [18, 19, 22, 23]. The quasi-neutrality of the beam is obtained by extracting positive ions and negative electrons from the same plasma source. Therefore, a high-speed self-neutralized plasma beam is produced, which miniaturizes the EP system since the neutralizer is not required [6].

A single-grid accelerator using the RF self-bias effect was first designed in [22], which extracted the ions and electrons quasi-simultaneously from the same inductively coupled plasma (ICP) source. The experimental results showed that this design has many disadvantages and limitations when applied to EP, such as low ion energy (<300 eV), ion sputtering, and low propellant utilization efficiency [6, 22, 24]. In order to solve these problems, an alternative method with a double-grid accelerator using the RF self-bias effect was proposed to extract a quasi-neutral plasma beam [18, 20, 25]. In the single-grid system, the RF voltage drop occurs mainly between the plasma and the grid. Ion acceleration occurring in front of the grid can cause severe ion sputtering [6, 24]. For the double-grid accelerator using the RF self-bias effect, the RF voltage drop occurs between the plasma and the two grids. Thus, the ion acceleration is mainly localized in the double-grid accelerator similar to the classical GIT, which effectively avoids ion sputtering [6]. In the double-grid system, the propellant utilization efficiency can be improved by optimizing the transparency of the acceleration grid to minimize the escape of neutral gas from the discharge chamber [1, 6]. The space charge limited current is almost doubled in the RF acceleration compared with the DC acceleration, which is attractive for EP to increase thrust [6, 26]. An experimental prototype named Neptune was performed with an RF power supply and the acceleration frequency was 4 MHz [18, 19, 27, 28]. The research indicates that the quasi-neutral beam was successfully extracted in RF acceleration [18–20]. The flux of electrons is highly anisotropic and directed along the direction of beam propagation when the double-grid accelerator is driven by an RF power supply. The measured IEDFs showed a multi-peak profile and the main peak almost disappears with a wide energy spread (100–800 eV) when the measured DC self-bias voltage is 300 V [18, 19]. In addition, the influence of different propellants on the plasma beam in RF acceleration is investigated [29]. The experimental and simulation results are consistent with the trend of the average ion velocity with the RF voltage amplitude. These experimental studies are beneficial for applying the technology of RF self-bias acceleration in the field of EP or other industries. However, there are many important contents worthy of in-depth study. The frequency of RF acceleration has a large effect on the accelerated beam [29, 30]. Therefore, the motivation of this work is to compare the characteristics of the plasma beam between the RF and DC acceleration in detail, and these results are measured at different RF acceleration frequencies.

In this paper, an experimental GIT prototype is designed which can operate in RF and DC acceleration. An RF power supply with a frequency of 7.8 MHz is used for RF acceleration, and a DC power with the same DC self-bias voltage of RF acceleration is applied for DC acceleration. Except for the acceleration power supply, other configurations of the two acceleration concepts are consistent, and the propellant gas is argon (Ar). Moreover, an RF-compensated four-grid retarding field energy analyzer (RFEA) is applied to diagnose the characteristics of the plasma beam. Next, the voltage waveforms between the double-grid are measured with different RF voltage amplitudes. The differences in beam characteristics between the RF and DC acceleration are investigated in detail, such as the floating potential, the spatial distribution of ion flux, and the ion energy distribution function (IEDF). In addition, the IEDFs of RF acceleration at different frequencies are compared.

The structure of this paper is organized as follows. The principles of RF and DC acceleration are illustrated in section 2. Experiment apparatus and procedures are described in section 3. The experimental results are discussed in section 4. Finally, a summary and further work are presented in section 5.

## 2. Principles of RF and DC acceleration

As shown in figure 1(a), two electrodes have unequal contact areas with the plasma in an asymmetric CCP system: the larger driven electrode K is biased with RF voltage via a blocking capacitor, and the smaller electrode A is grounded directly. Asymmetry refers to the unequal area of the two electrodes connected to the plasma. The capacitor is used to prevent DC currents from being generated in the circuit, ensuring that the time-average electron and ion currents to the electrode are equal. Then, there will be a significant shift of the voltage waveform between electrodes K and A due to the different response of ions and electrons to the time-oscillating electric field, which is commonly called the RF self-bias effect [6, 26]. As shown in figure 1(b), the value of this offset is known as the DC self-bias voltage ($V_{DC}$). For analysis, assuming that the voltage signal from the RF generator is

$$V(t) = V_{RF} \sin \omega t, \tag{1}$$

where $V_{RF}$ is the amplitude of the RF voltage, and $\omega$ is the

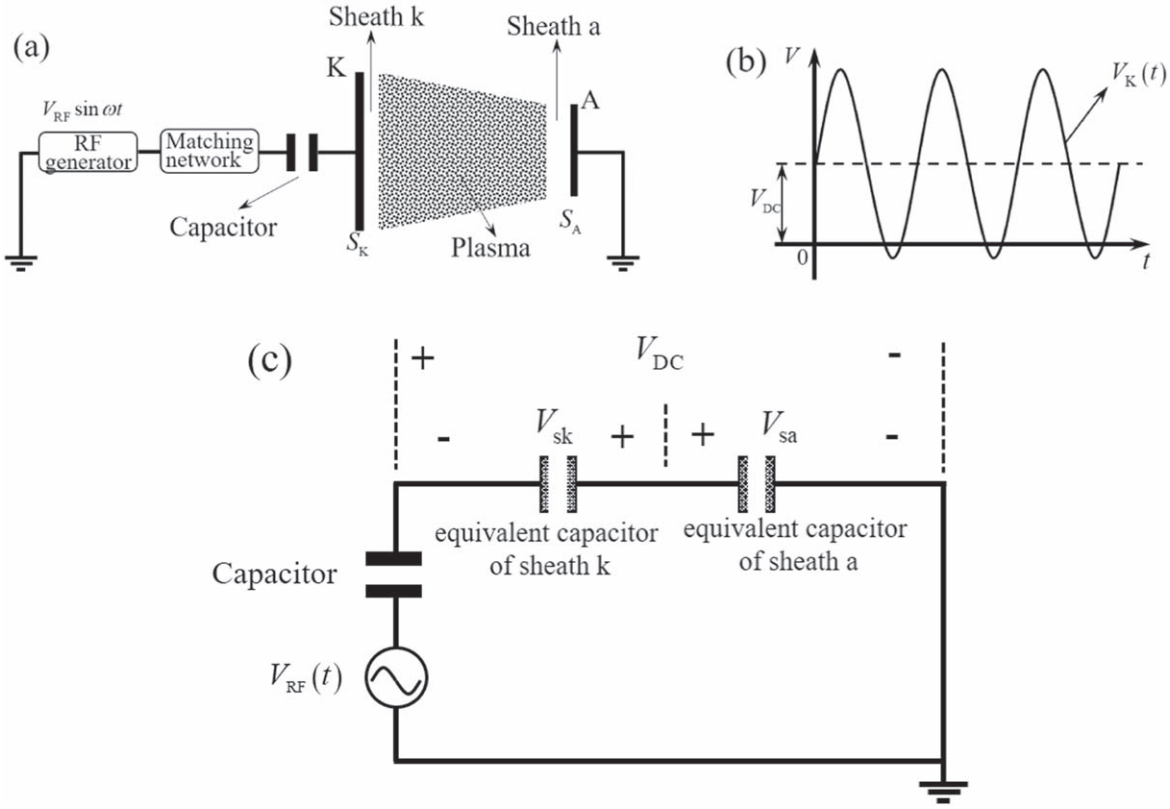


**Figure 1.** (a) Schematic of the asymmetrical CCP model; (b) the voltage waveform on electrode K and DC self-bias voltage; (c) capacitive voltage divider model of DC self-bias voltage. $S_K$ and $S_A$ are the areas of electrode K and electrode A in contact with the plasma, respectively. $V_{sk}$ and $V_{sa}$ are voltage drops on sheath $k$ and sheath $a$, respectively.

frequency of the RF voltage. According to the theory of the RF self-bias effect, the voltage between electrodes K and A is expressed as [26]

$$V_K(t) = V_{DC} + V_{RF}\sin\omega t. \tag{2}$$

Therefore, $V_K(t)$ is a sinusoidal waveform with a shift value, and it consists of DC and AC components. The DC component voltage is the DC self-bias voltage ($V_{DC}$).

The magnitude of the DC self-bias voltage is influenced by the area of the two electrodes in contact with the plasma. As illustrated in figure 1(c), the voltage drops across the two sheaths (sheath $k$ and $a$) are calculated according to the capacitive voltage divider model of asymmetric CCP. Hence, the DC self-bias voltage can be presented as [26]

$$V_{DC} = \overline{V}_{sa} - \overline{V}_{sk}, \tag{3}$$

where $\overline{V}_{sa}$ and $\overline{V}_{sk}$ are the time-averaged voltage drops across 'sheath $a$' and 'sheath $k$', respectively. According to the self-consistent solution, the voltage drops are estimated as follows [26, 31]

$$\frac{\overline{V}_{sa}}{\overline{V}_{sk}} \approx \left(\frac{S_K}{S_A}\right)^q, \tag{4}$$

where $1 \leqslant q \leqslant 4$, $S_K$ and $S_A$ are the areas of electrodes K and A in contact with the plasma, respectively. Therefore, almost the whole of the RF voltage is dropped across the 'sheath a' when the asymmetry is extremely obvious (i.e. $S_K \gg S_A$), and the value of the DC self-bias voltage ($V_{DC}$) is close to the RF voltage amplitude ($V_{RF}$). Theoretically, there is a linear relationship between $V_{DC}$ and $V_{RF}$ according to equations (3) and (4). The actual situation is more complicated, and the relationship needs to be determined by specific experiments [26].

The RF self-bias effect can be used to generate quasi-neutral beams. As illustrated in figure 2, a double-grid accelerator (ion optical system) is placed at the exit of a plasma source, which is similar to the classical GIT as shown in figure 3 [1]. As shown in figure 2(a), the screen grid $G_S$ is driven by RF power supply via a blocking capacitor, and the acceleration grid $G_A$ is grounded directly. In this paper, the screen grid and the acceleration grid are the grids closer and further away from the plasma source, respectively, which are named following the classical GIT. The screen grid is directly in contact with the plasma, while the acceleration grid can only contact the plasma through apertures in the screen grid. The contact area between the plasma and the two grids is not equal, resulting in an asymmetry. Therefore, the DC self-bias voltage is formed on grid $G_S$. In this RF-biased grid system, the plasma sheath in front of the double-grid oscillates with time, as shown in figure 2(a), and the plasma potential at the center of the hole of the screen grid is shown in figure 2(b). The oscillating sheath can accelerate the ions continuously, but the electrons are strongly limited until the sheath is close to zero. Then, a self-neutralized plasma beam is generated from the same plasma source, and the external neutralizer is not necessary. In this process, the oscillating sheath is the key to the extraction of the quasi-neutral plasma beam, which is

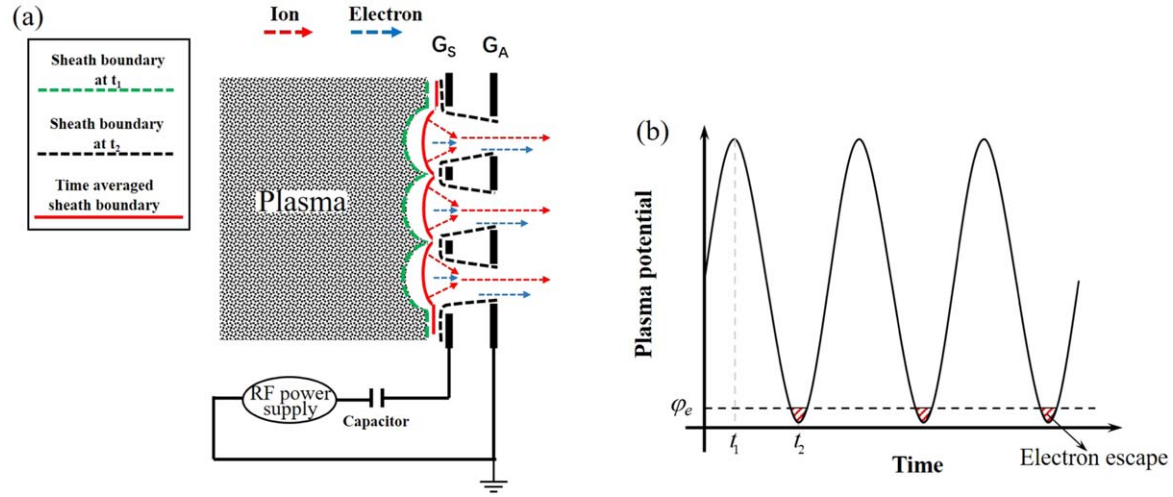


**Figure 2.** Principle diagram of RF acceleration with a double-grid accelerator. (a) Extraction of electrons and ions by the oscillating sheath. (b) Plasma potential and electron extraction moment. $\varphi_e$ is the plasma potential corresponding to the sheath collapse.

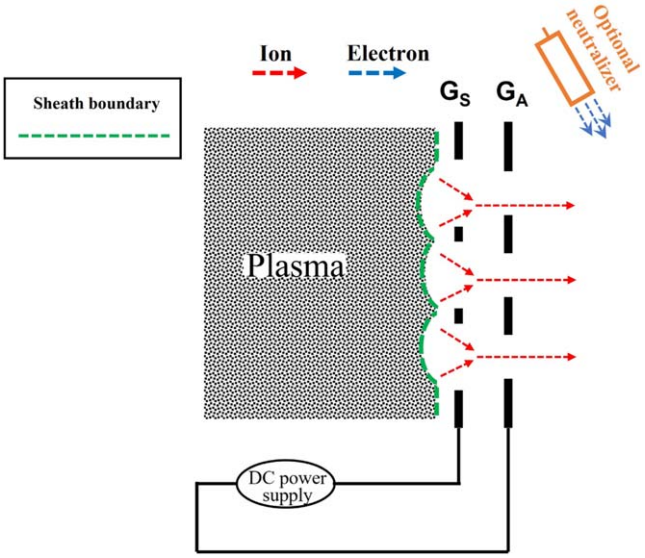


**Figure 3.** Principle diagram of DC acceleration with double-grid accelerator.

mainly decided by the amplitude of the voltage and the frequency of the RF power. The ion plasma frequency $f_{\text{ion}}$ and electron plasma frequency $f_e$ characterize the highest frequency at which ions and electrons can respond to the electric field oscillation, respectively. $f_{\text{ion}}$ and $f_e$ are estimated by [26]

$$f_{\text{ion}} = \frac{1}{2\pi}\sqrt{\frac{e^2 n_0}{\varepsilon_0 M_{\text{ion}}}}$$
$$f_e = \frac{1}{2\pi}\sqrt{\frac{e^2 n_0}{\varepsilon_0 m_e}}, \quad (5)$$

where $e$ is the elementary charge, $M_{\text{ion}}$ is the ion mass, $m_e$ is the electron mass, $\varepsilon_0$ is the vacuum permittivity, and $n_0$ is the plasma density. Both the ion plasma frequency and the electron plasma frequency are affected by the plasma density which is maintained by a constant ICP discharge power in this research.

By contrast, the principle of DC acceleration is well known, as shown in figure 3. The screen grid is connected to a DC power supply, and the acceleration grid is grounded. Therefore, there is only one DC component of the voltage between the double-grid. A stable DC plasma sheath is distributed in front of the double-grid, and only ions are accelerated to form a positive beam. Therefore, in the classical DC acceleration system, an additional neutralizer is needed to provide electrons for space charge compensation, then a quasi-neutral plasma beam is formed. For the convenience of comparing the characteristics and performance, the DC component voltage between the double-grid of RF and DC acceleration is equal, which is the same as that in the [18, 25].

## 3. Experimental apparatus and procedures

The schematic diagram of the principle prototype is illustrated in figure 4. Compared with the classical RF GIT, the concept of RF acceleration has a strong technical inheritance. The plasma discharge chamber is a cylindrical cavity, and both the diameter and axial length are 6 cm. An ICP source is excited by an RF antenna which is separated from the plasma source by a 2 mm thick cylindrical alumina ceramic and powered by an RF power of 13.56 MHz. To reduce the power reflection, the matcher system is applied to match the impedance between the RF power and the plasma load. Moreover, the Ar gas is uniformly fed into the discharge chamber through a ceramic gas injector. The full scale of the gas mass flow controller is 10 sccm (accuracy: ±(0.4%RD + 0.2%FS)).

The double-grid ion accelerator is located at the exit of the discharge chamber. As shown in figure 5, its main components include a ceramic isolator, two grids with coaxial apertures, and two bias boards. The insulated ceramic sheet is positioned between the two grids to maintain grid spacing and the bias boards are used to apply voltage to the grids. The grid is made of molybdenum and the apertures are manufactured by electrical discharge machining.

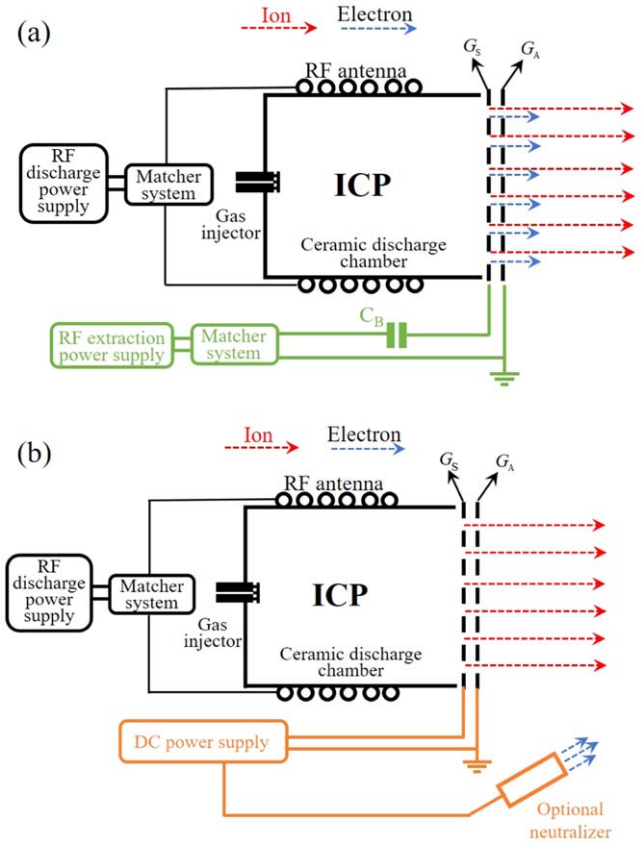


**Figure 4.** Schematic diagram of the experimental prototype. (a) The RF acceleration with neutralizer-free. (b) The DC acceleration with a neutralizer. (a) and (b) are called 'RF acceleration mode' and 'DC acceleration mode', respectively.

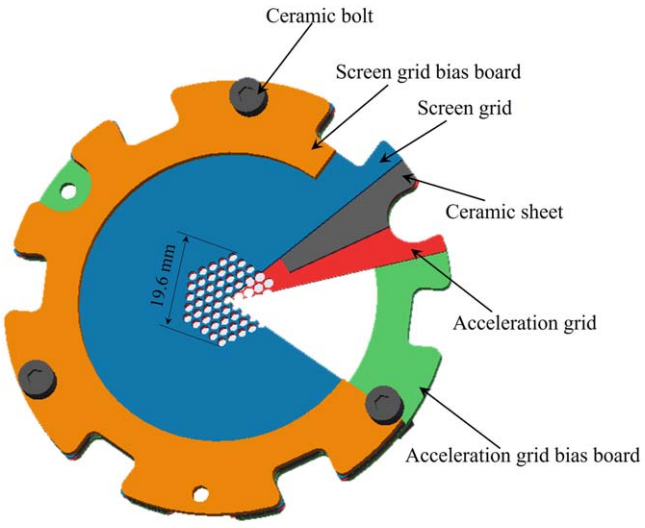


**Figure 5.** Schematic diagram of the double-grid accelerator.

The apertures on the two grids are hexagonally arranged, and the maximum diameter of the extractable beam region of the double-grid is 19.4 mm. The diameter of the ICP discharge chamber is larger than that of the grid aperture region to ensure that the plasma parameters in front of the grid apertures are as uniform as possible and to reduce the influence of the plasma properties on the spatial distribution of the downstream beam parameters. In our experimental double-grid accelerator, the number of apertures for each grid is 61, and the distance of each aperture is 2.2 mm. The distance between $G_S$ and $G_A$ depends on the insulation ceramic sheet (0.85 mm in thickness). The other dimensions of the double-grid accelerator are listed in table 1.

**Table 1.** Grid parameters.

| Parameters | Values |
|---|---|
| $G_S$ aperture diameter (mm) | 2.0 |
| $G_S$ thickness (mm) | 0.5 |
| $G_A$ aperture diameter (mm) | 1.8 |
| $G_A$ thickness (mm) | 0.8 |
| Aperture axis spacing (mm) | 2.2 |
| Grid spacing (mm) | 0.85 |
| Number of apertures | 61 |

$G_S$ refers to the grid close to the plasma source.
$G_A$ refers to the grid far away to the plasma source.

In RF acceleration mode, as shown in figure 4(a), grid $G_S$ is driven by an RF voltage via a blocking capacitor $C_B$ (0.22 $\mu$F), and grid $G_A$ is connected directly to the ground. In DC acceleration mode, as shown in figure 4(b), the double-grid accelerator is driven by a DC voltage, and an additional neutralizer is necessary for providing electrons. We adopt a hot cathode as the neutralizer in this work. The RF and DC acceleration modes share a common ICP source in this research, different operating modes can be realized by changing the type of driven power supply applied to the double-grid accelerator. To ensure consistency of the plasma source during the test, the RF power of ICP remained at 45 W and the gas flow rate was 4 sccm. In RF acceleration mode, different DC self-bias voltages are obtained by changing the power of the RF extraction power supply, and the real voltages are determined by directly measuring the voltage waveform between the double-grid. A photograph of the designed thruster prototype is shown in figure 6.

A schematic of the prototype test facility is shown in figure 7. The vacuum chamber is composed of a cubic chamber with a volume of 0.512 $cm^3$ at one end and a cylindrical chamber of 30 cm in length and diameter at the other. The vacuum pump system consists of a turbopump (27 000 l $min^{-1}$), a rough pump, and a maintenance pump. The base pressure in the low range of $10^{-4}$ Pa ($10^{-6}$ Torr) is achievable after 50–60 min of operation of the vacuum pump system. The Ar flow rate of 0.5–10 sccm induced the chamber pressure of $2.1 \times 10^{-3}$–$2.7 \times 10^{-2}$ Pa ($1.6 \times 10^{-5}$–$2.0 \times 10^{-4}$ Torr), respectively. The thruster prototype is fixed in the vacuum chamber and connected to the external power and gas supply systems through vacuum-sealed feedthroughs.

The facility is equipped with an RF-compensated four-grid RFEA for measuring beam parameters. RFEAs have been widely used in plasma diagnostics [32–34]. In this research, the RFEA is introduced to measure the beam parameters including floating potentials, IEDFs, and ion fluxes. To facilitate descriptions, the $x$-axis and $z$-axis are

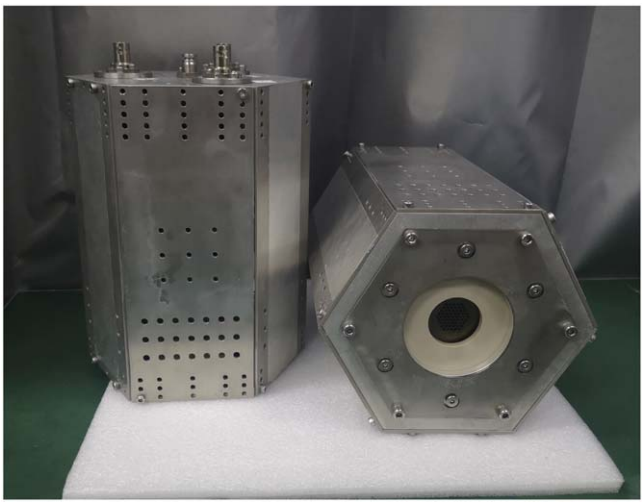

**Figure 6.** A photo of the thruster prototype designed for RF and DC acceleration.

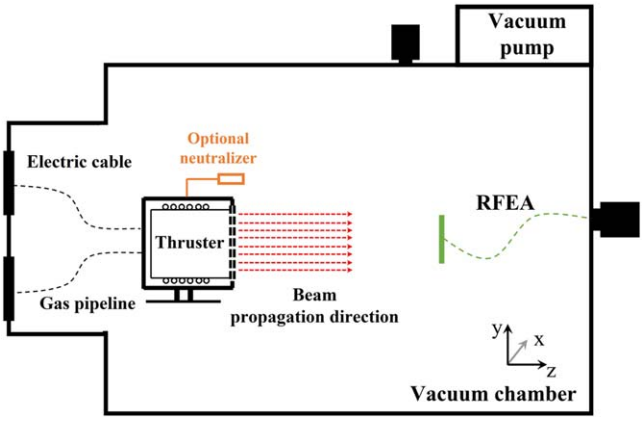


**Figure 7.** Schematic diagram of the experimental device. The thruster prototype is fixed in the vacuum chamber. The additional neutralizer (shown in orange line) can be turned on or off independently.

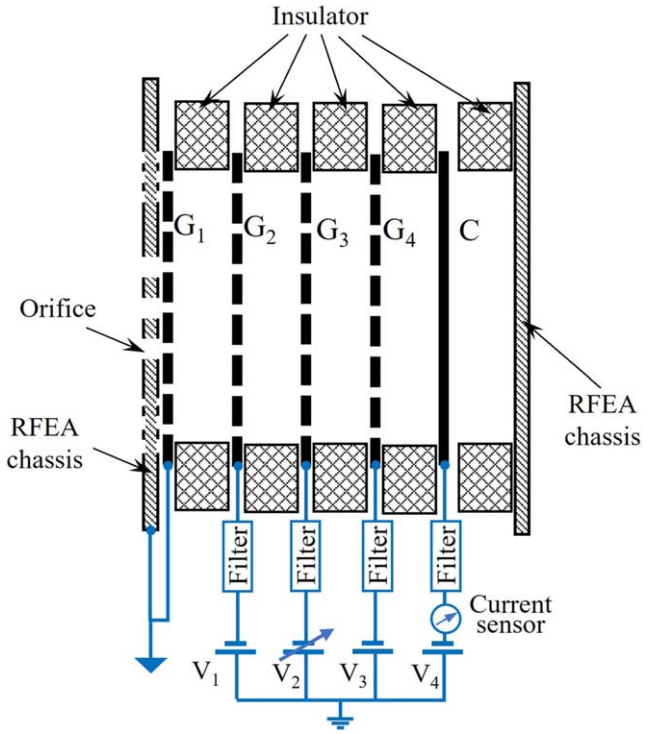


**Figure 8.** Schematic of the four-grid RFEA structure. The detected particles enter the RFEA through the orifices.

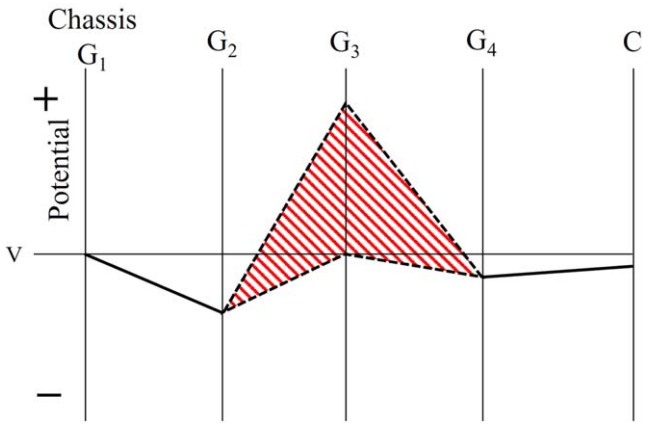


**Figure 9.** The bias configuration of RFEA for positive ion distribution.

defined as the radical and propagation directions of the accelerated beam, respectively, as shown in figure 7. The $z$-axis is at the centerline of the beam, and $z = 0$ is defined as the exit of the double-grid accelerator. The RFEA probe can be moved along the $x$-axis to measure the radial distribution of beam parameters. For all tests, the RFEA probe is located downstream of the beam at $z = 15$ cm. The entrance surface of the RFEA probe is perpendicular to the beam propagation direction.

The structure of the RFEA is described in figure 8. The orifice faces the beam plasma that allows the samples of diagnostic particles to enter the RFEA for analysis. Grid $G_1$ covers the orifices in the backside to prevent plasma from forming inside the RFEA [32]. When the measured particles are ions, the RFEA grid potential configuration is shown in figure 9. Grid $G_2$ is negatively biased relative to $G_1$ to repel any electrons entering the analyzer. Grid $G_3$ with positive potential scanning is applied to distinguish positive ions based on their energy. Collector C is used to collect and record the ion currents. Grid $G_4$, located between $G_3$ and C, is usually biased 10 V more negative than C to prevent secondary electrons from escaping from collector C, allowing for accurate measurement results. $G_1$, $G_2$, $G_3$ and $G_4$ are of the same size with the apertures of 20 $\mu$m in diameter. The first derivative of the *I–V* characteristics of collector C is proportional to the IEDF. When the sensor is at a floating potential, the electron and ion currents that reach the RFEA are equal. The total ion flux of the collector is calculated by trapezoidal integration of the ion energy distribution. The auxiliary software will automatically process the measurement data, presenting floating potential, IEDF, and ion flux ($\Gamma_{\perp ion}$).

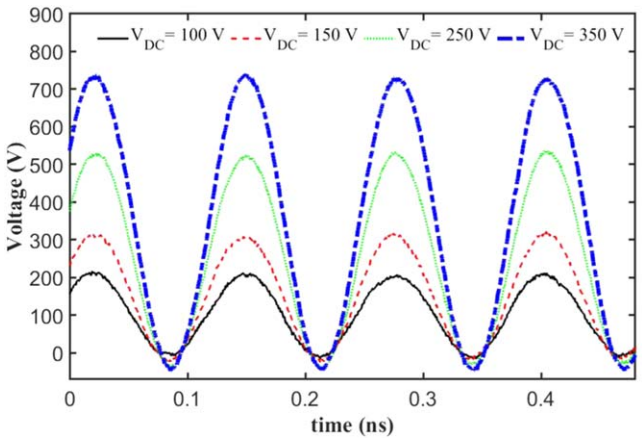


**Figure 10.** Voltage waveforms were measured between double-grid under different RF voltages. $V_{DC}$ is 100 V, 150 V, 250 V, and 350 V corresponding to $V_{RF}$ of 117 V, 174 V, 291 V, and 398 V, respectively.

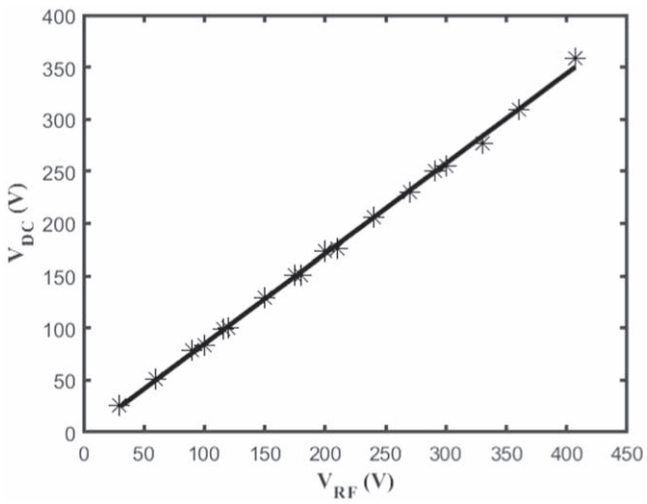


**Figure 11.** The DC self-bias voltage as a function of the RF voltage amplitude.

## 4. Experimental results

### *4.1. DC self-bias voltage and beam formation*

In the concept of RF acceleration, the formation of the RF self-bias effect is a prerequisite for achieving an accelerated quasi-neutral beam. As described in section 2, a DC self-bias voltage is generated under the RF self-bias effect. Therefore, the first consideration is to determine whether the DC self-bias voltage develops at different RF voltages by measuring the voltage waveform between the double-grid.

The measurements were recorded by an oscilloscope, as demonstrated in figure 10. DC self-bias voltages ($V_{DC}$) are 100 V, 150 V, 250 V, and 350 V corresponding to the RF voltage amplitudes ($V_{RF}$) of 117 V, 174 V, 291 V, and 398 V, respectively. Different sinusoidal voltage waveforms between the double-grid are obtained with a shift toward the positive value, which is similar to figure 1(b). The value of this shift is the DC self-bias voltage $V_{DC}$. As a result, the RF self-bias effect is successfully formed in the prototype test. Furthermore, figure 10 reveals that the DC self-bias voltage increases with the amplitude of the RF acceleration voltage. The measured DC component $V_{DC}$ as a function of $V_{RF}$ is shown in figure 11. A linear relationship is obtained as $V_{DC} \approx 0.87 V_{RF}$, which is close to the theoretical estimation of the DC self-bias voltage in low-pressure asymmetric CCP [26]. In addition, the extracted beam becomes obvious as the RF acceleration voltage increases. An experimental photo of the extracted beam with the DC self-bias voltage of 350 V is shown in figure 12, and a stable and well-focused plasma beam was observed.

### *4.2. Spatial potential of the beam*

Although the above results demonstrate the formation of the RF self-bias effect, it is not enough to prove that both electrons and ions are extracted. The co-extracted electrons and ions are charge-compensated in the downstream beam to achieve self-neutralization. This can be investigated by

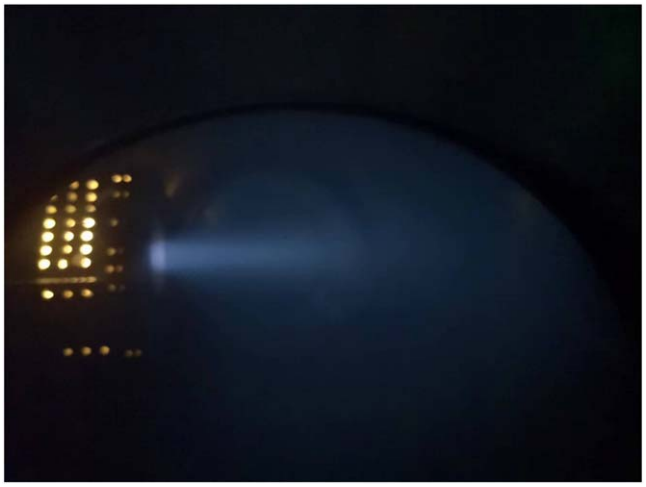

**Figure 12.** A photo of the beam in RF acceleration mode.

measuring the floating potential of the beam plasma [18, 19, 26]. For comparison, the following three operation cases of the prototype were designed.

- (A) The double-grid accelerator is RF-biased, and the prototype operates without a neutralizer (RF acceleration mode).
- (B) The double-grid accelerator is DC-biased, and the prototype operates with an additional neutralizer (DC acceleration mode).
- (C) The double-grid accelerator is DC-biased, and the prototype operates without a neutralizer.

In all three cases, the same ICP source and double-grid accelerator were used, but the beam was extracted by different powers, as shown in figure 4.

The spatial floating potential measured as a function of the DC component voltage in three cases is shown in figure 13. For case (C), as shown in the red line in figure 13(a), the results indicate that the spatial floating potential is almost comparable to the DC component voltage.

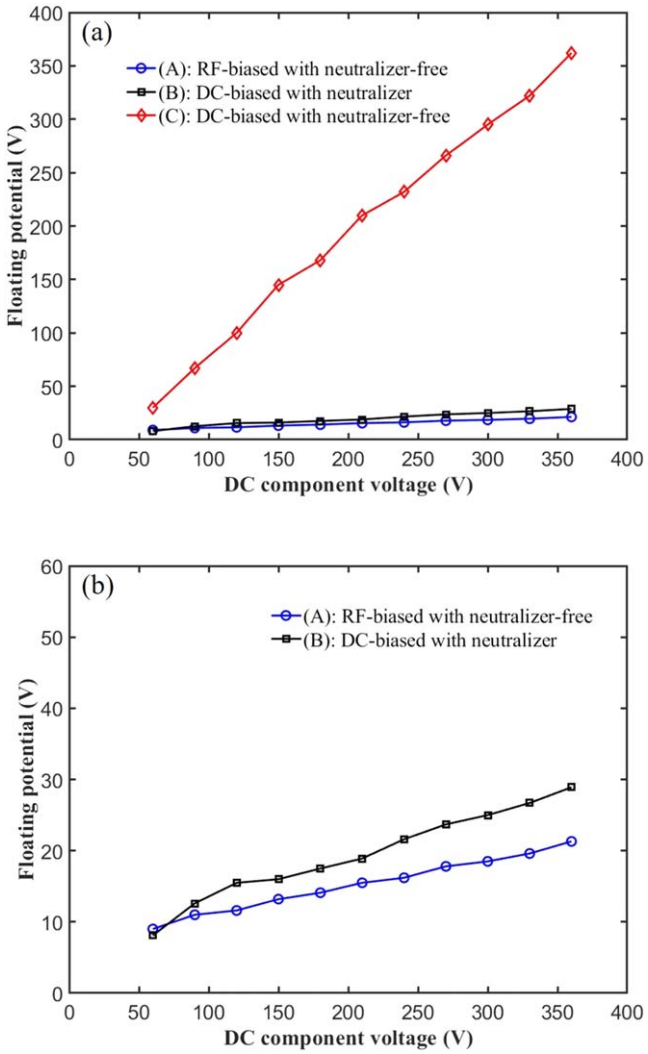


**Figure 13.** Floating voltage as a function of the DC component voltage between the double-grid. The results of cases (A), (B), and (C) are shown in (a). The details of cases (A) and (B) are compared in (b). The RFEA probe was placed at $z = 15$ cm in the center of the beam.

This is because only ions are extracted from the ICP source, and there are no electrons to compensate for the positive charge in this case. The RFEA probe is charged by positive ions and represents a high floating potential. While in case (B), there is an additional neutralizer to emit electrons, which allows the spatial ion charge to be compensated. Consequently, the spatial floating potential is maintained at a low level (<29 V), as shown in the blue line in figure 13(b). The results of case (A) show that the spatial floating potential is maintained at a low level (<21 V), which is similar to case (B), as shown in the black line in figure 13(b). It indicates that the accelerated beam is self-neutralized in RF acceleration mode because the continuously accelerated ions and the intermittently diffused electrons are extracted quasi-simultaneously.

In addition, by comparing cases (A) and (B), the floating potential measured in RF acceleration mode is slightly lower than that in DC acceleration mode, and this difference

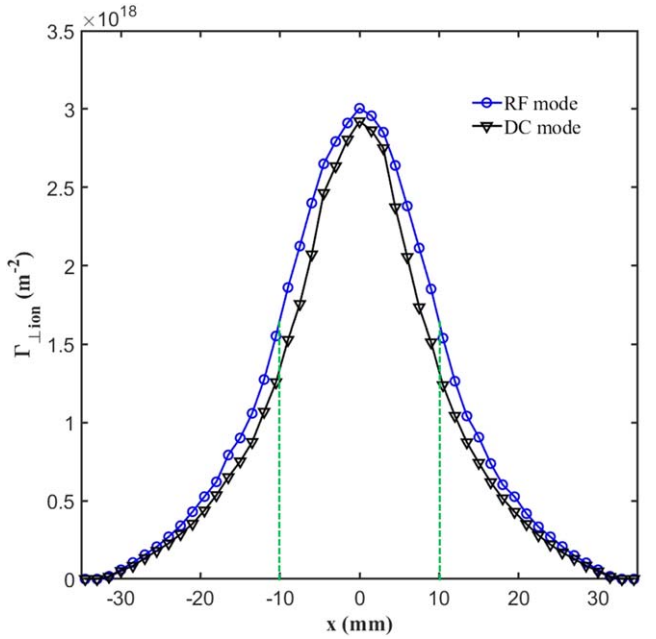


**Figure 14.** Spatial distribution of ion flux. The ion flux is measured when the DC component voltage between the double-grid is 250 V. The RFEA probe was placed at $z = 15$ cm, and the data at each point was the average of ten measurements.

increases with the acceleration voltage. It is shown that the effect of the charge-compensated is more efficient in RF self-neutralized acceleration mode. That is because the ions and electrons are both extracted from the double-grid system and the motion of electrons shows significant anisotropy. It leads the electrons to be co-extracted with the ions in the same direction, which can promote the charge compensation of electrons and ions. In contrast, electrons are emitted from an external neutralizer in DC acceleration mode, it is not synchronized with the extraction of ions.

### *4.3. Spatial distribution of ion flux*

The ion flux extracted in different acceleration modes is an important parameter to evaluate the acceleration performance. The spatial distribution of beam ion flux is recorded as the RFEA probe moves along the radial ($x$-axis) direction of the beam, as shown in figure 7. The results are shown in figure 14 when the DC component voltage between the double-grid is 250 V. In both RF and DC acceleration modes, the maximum ion flux is at the center of the beam and the ion flux decreases gradually from the center to the edge of the beam. At $x = \pm 10$ mm, corresponding approximately to the boundary of the grid aperture area whose maximum diameter is 19.6 mm, the ion flux drops to approximately half of that at the center of the beam.

A coefficient $\lambda$ is introduced to compare the ion fluxes measured in both RF and DC acceleration modes as

$$\lambda = \frac{\Gamma_{\perp \mathrm{RF}}(x)}{\Gamma_{\perp \mathrm{DC}}(x)}, \tag{6}$$

where $\Gamma_{\perp \mathrm{RF}}(x)$ and $\Gamma_{\perp \mathrm{DC}}(x)$ are the ion fluxes measured in RF and DC acceleration modes at the position of $x$, respectively.

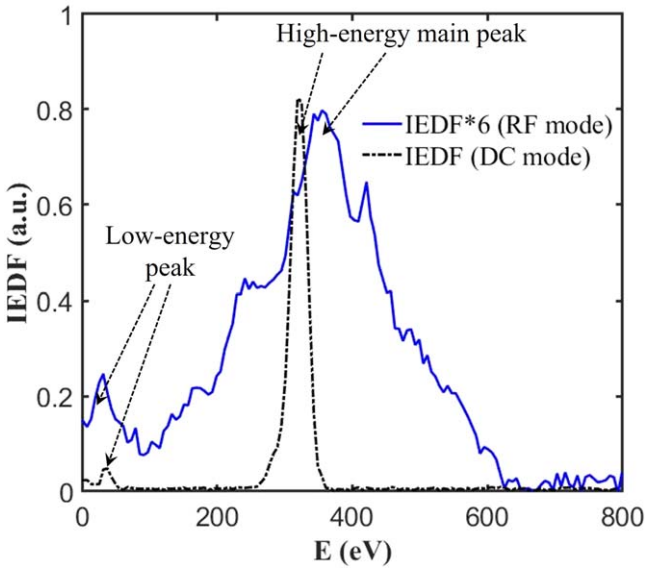


**Figure 15.** IEDFs measured in RF and DC acceleration modes. The DC component voltage between the double-grid is 300 V.

The average value of $\lambda$ in the range of $(-30, 30)$ is calculated to be 1.17, which indicates that $\Gamma_{\perp \mathrm{ion}}$ in RF acceleration mode is higher than that in DC acceleration mode. This may be because electrons are extracted periodically from the oscillating sheath in RF mode. Although the DC component voltage is equal, it is a stable DC ion sheath in DC acceleration mode and an oscillating 'DC + RF' sheath in RF acceleration mode [18]. Electrons are repulsive in the DC ion sheath while electrons are allowed to pass through the double-grid accelerator for the oscillating 'DC + RF' sheath. Therefore, in RF acceleration mode, the extracted electrons result in a nonzero, time-averaged electron density between the screen and accelerator grids. Then the space charge within the sheath will reduce, which allows more ions to be extracted from the plasma source [6, 26]. In addition, the beam flatness can be calculated as [35]

$$\alpha = \frac{\bar{\Gamma}_{\perp}}{\Gamma_{\perp \max}}, \tag{7}$$

where $\bar{\Gamma}_{\perp}$ and $\Gamma_{\perp \max}$ are the measured average and maximum values of ion fluxes, respectively. According to the measurements in figure 14, it is 0.36 in RF and 0.33 in DC mode. The beam is slightly more uniform in RF mode than in DC mode.

### *4.4. Ion energy distribution*

IEDFs provide a clear overview of the acceleration effect of the beam ions. For the IEDF measurements, the RFEA probe is fixed at the beam center position of $z = 15$ cm. Figure 15 shows the results in both RF and DC acceleration modes when the DC component voltage between the double-grid is 300 V. It is indicated that there are significant differences between RF and DC acceleration modes. In DC acceleration mode, as shown in the black line in figure 15, the IEDF has two distinguishable ion energy regions with a narrow energy spread: the low-energy ion region and the high-energy ion region. The energy spread of low-energy and high-energy ions is approximately 30 eV and 80 eV, respectively. The high-energy ion distribution tends to become virtually monoenergetic. While in RF acceleration mode, the IEDF is roughly divided into two regions with a wide energy spread and multi-peaked profile. The low-energy ions created downstream are roughly located in the range of 0–100 eV. The high-energy ions accelerated by the double-grid are located between about 100 and 630 eV.

The oscillatory sheath is one reason for the complicated IEDF. In RF acceleration mode, the average ion transit time through the double-grid can be estimated by [30]

$$\Delta t = \sqrt{\frac{2L^2 M_{\mathrm{ion}}}{eV_{\mathrm{DC}}}}, \tag{8}$$

where $M_{\mathrm{ion}}$ is the ion mass, $e$ is the elementary charge (single charged ions are supposed in this research), and $V_{\mathrm{DC}}$ is the DC self-bias voltage. $L$ is the effective intergrid separation distance calculated by

$$L = \sqrt{(l_{\mathrm{g}} + t_{\mathrm{S}})^2 + r_{\mathrm{S}}^2}, \tag{9}$$

where $l_{\mathrm{g}}$ is the physical intergrid separation distance, $t_{\mathrm{S}}$ is the thickness of grid $G_{\mathrm{S}}$, and $r_{\mathrm{S}}$ is the radius of the apertures on grid $G_{\mathrm{S}}$. Ar is used in this test, and the grid parameters are listed in table 1. For the DC self-bias voltage of 300 V, $\Delta t$ is about 0.07 ns calculated by equations (8) and (9). The period of the 7.8 MHz RF accelerating voltage is 0.13 ns, which is comparable to $\Delta t$. Therefore, ions tend to be affected by the varying RF voltages and oscillatory plasma sheath [36]. The energy gained by an ion while crossing the sheath depends on the phase of the RF modulation.

The IEDFs measured at different acceleration voltages in DC and RF acceleration modes are shown in figures 16(a) and (b), respectively. In both acceleration models, the main peak of the IEDF moves toward the high-energy region as the acceleration voltage increases. The difference is that the energy spread of high-energy ions is almost constant in DC acceleration mode, but widens with the increase of the acceleration voltage in RF acceleration mode. This is because, in the range of $V_{\mathrm{DC}} = 150$–$350$ V, the $\Delta t$ calculated by equation (8) is comparable to the RF period. For a higher $V_{\mathrm{DC}}$, the voltage range of ions accelerated by the oscillating sheath is increased, resulting in a widened ion energy distribution.

The frequency of the RF acceleration voltage is one of the key parameters affecting the characteristics of the beam ions. The IEDFs measured at the frequencies of 3.9 and 7.8 MHz under the same DC self-bias voltage of 300 V are shown in figure 17. It is indicated that the energy spread of the high-energy ion peak at high frequency (7.8 MHz) of approximately 100–630 eV is narrower than that at low frequency (3.9 MHz) of approximately 80–710 eV. The high-energy ions are more concentrated and the main peak is more pronounced at high frequency (7.8 MHz). While at low frequency (3.9 MHz), the high-energy ions are more evenly distributed over the whole high-energy region and the main

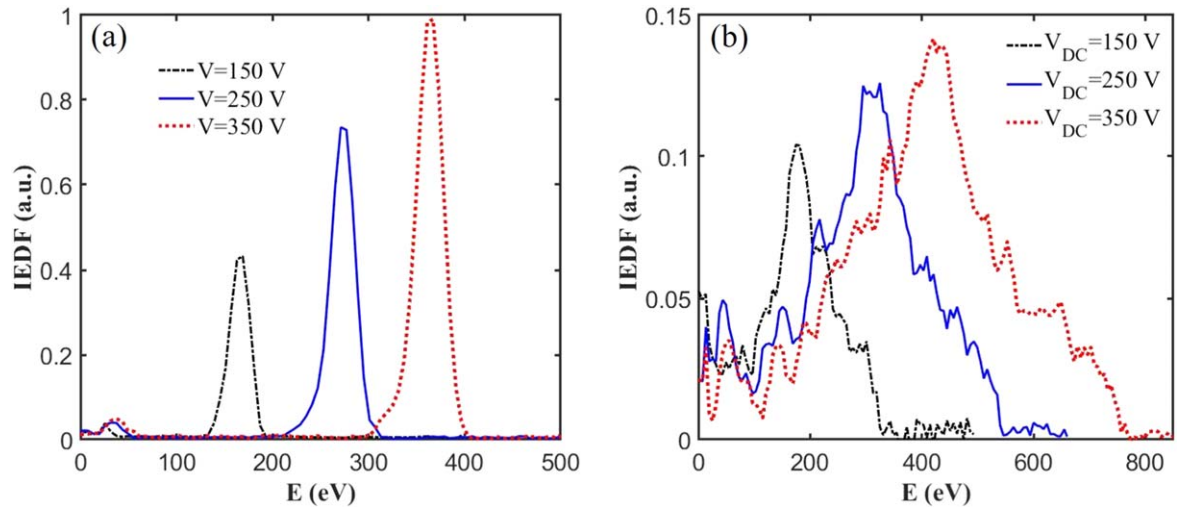


**Figure 16.** IEDFs measured at different DC component voltages: 150 V, 250 V and 350 V. The results in DC and RF acceleration modes are shown in (a) and (b), respectively.

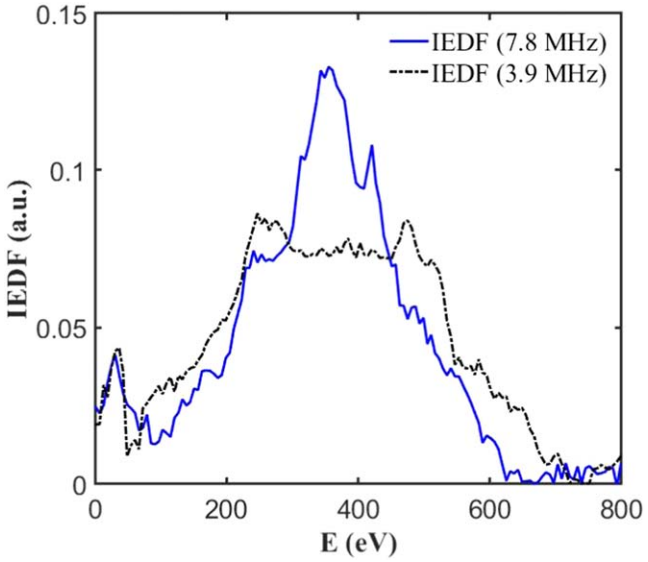


**Figure 17.** IEDFs measured at 7.8 and 3.9 MHz. The data was measured when the DC component voltage between the double-grid is 300 V.

peak is almost indiscernible, which is similar to the experimental results in [19] with an acceleration frequency of 4 MHz. These results are consistent with the theoretical analysis and simulation results that the ion energy spread is inversely proportional to the applied frequency [26, 29].

## 5. Conclusion

Experimental GIT prototypes with RF-biased and DC-biased double-grid accelerators have been designed respectively to investigate the different characteristics of the plasma beams. Argon is the working gas. The voltage waveforms between the double-grid in RF acceleration mode have been measured with different RF voltage amplitudes. When the frequency of the RF acceleration voltage is 7.8 MHz, the floating potential, the spatial distribution of ion flux, and the IEDF of the extracted beams have been analyzed by a four-grid RFEA and compared in RF and DC acceleration modes.

The experimental results show that the RF self-bias effect has been successfully formed, and the different sinusoidal voltage waveforms with a shift value of the DC self-bias voltage have been obtained at different amplitudes of the RF acceleration voltage. The DC self-bias voltage varies linearly with the amplitude of the RF acceleration voltage, about $V_{DC} \approx 0.87 V_{RF}$, which is consistent with the theoretical estimation of the RF self-bias effect in low-pressure asymmetric CCP. In addition, a stable and well-focused plasma beam has been observed.

The measured floating potentials indicate that the space charge of the plasma beam is adequately compensated in both RF and DC acceleration modes, which means that the ions and electrons are co-extracted from the same ICP source in RF acceleration mode. However, the floating potential in RF acceleration mode is slightly lower than that in DC acceleration mode, and their difference will gradually increase with the DC component of the acceleration voltage. In both RF and DC acceleration modes, the ion flux decreases gradually from the center to the periphery of the plasma beam. The average ion flux in RF acceleration mode is about 1.17 times larger than that in DC acceleration mode, which illustrates that the ions can be extracted more effectively in RF acceleration mode. Due to the influence of RF phase modulation of the oscillating sheath, the IEDF of the high-energy ions is multi-peaked and wide in RF acceleration mode; while in DC acceleration mode, the IEDF of the high-energy ions is single-peaked with a narrow energy spread. In addition, the main peak of IEDF moves toward the high-energy region as the acceleration voltage increases in both modes, but the energy spread of the high-energy ions will increase in RF acceleration mode. Finally, comparing the IEDFs with the frequencies of 3.9 and 7.8 MHz, it is found that the energy spread of the high-energy ions is narrower and the main peak is more pronounced at a higher frequency.

The concept of extracting a quasi-neutral plasma beam from a single plasma source has great prospects in space propulsion. In particular, a neutralizer is not required in RF acceleration mode, which contributes to miniaturizing the EP system. Further experimental research will be carried out, such as the effect of different RF acceleration frequencies, the optimal design of the double-grid accelerator.

## Acknowledgments

This work was supported by Shenzhen Technology Projects (No. ZDSYS201707280904031) and the China Postdoctoral Science Foundation (No. 2022M710977).

## References

[1] Goebel D M and Katz I 2008 *Fundamentals of Electric Propulsion: Ion and Hall thrusters* (New York: Wiley)
[2] Hey F G 2018 *Micro Newton Thruster Development* (Berlin: Springer)
[3] Dale E, Jorns B and Gallimore A 2020 *Aerospace* **7** 120
[4] Lev D *et al* 2019 *Acta Astronaut.* **159** 213
[5] Herman D *et al* 2018 *Int. Electric Propulsion Conf.* (Boston, MA: IEPC)
[6] Rafalskyi D and Aanesland A 2016 *Plasma Sources Sci. Technol.* **25** 043001
[7] Lev D *et al* 2015 *Proc. of the 34th Int. Electric Propulsion Conf. (IEPC)* (Japan: IEPC) pp 6–10
[8] Hua Z W *et al* 2022 *Plasma Sci. Technol.* **24** 074004
[9] Hu Y L *et al* 2020 *Plasma Sci. Technol.* **22** 015401
[10] Wu Z W *et al* 2020 *Plasma Sci. Technol.* **22** 094014
[11] Yang Z Y *et al* 2022 *Plasma Sci. Technol* **24** 074006
[12] Geng J Y *et al* 2020 *Plasma Sci. Technol* **22** 094012
[13] Zhao Y Z *et al* 2022 *Plasma Sci. Technol.* **24** 074001
[14] Ou Y *et al* 2022 *Phys. Plasmas* **29** 013506
[15] Fu Y F *et al* 2021 *Plasma Sci. Technol.* **23** 104005
[16] Wu P *et al* 2020 *Plasma Sci. Technol.* **22** 094008
[17] Lafleur T *et al* 2014 *Plasma Sources Sci. Technol.* **24** 015005
[18] Rafalskyi D and Aanesland A 2014 *J. Phys. D: Appl. Phys.* **47** 495203
[19] Rafalskyi D and Aanesland A 2015 Characterization of a neutralizer-free gridded ion thruster *Int. Electric Propulsion Conf., IEPC–2015* (Boston, MA: IEPC)
[20] Rafalskyi D and Aanesland A 2017 A neutralizer-free gridded ion thruster embedded into a 1u cubesat module *Proc. of the 35th Int. Electric Propulsion Conf., Atlanta, GA, USA* (Boston, MA: IEPC) pp 8–12
[21] Lafleur T *et al* 2019 Radio-frequency biasing of ion thruster grids, *36th Int. Electric Propulsion Conf., Electric Rocket Propulsion Soc. Paper IEPC-2019-362* (Boston, MA: IEPC) 2019
[22] Dudin S and Rafalskyi D 2009 *EPL (Europhys. Lett.)* **88** 55002
[23] Dedrick J *et al* 2017 *Phys. Plasmas* **24** 050703
[24] Dudin S and Rafalskyi D 2012 *Rev. Sci. Instrum.* **83** 113302
[25] Rafalskyi D and Aanesland A 2015 *Phys. Plasmas* **22** 063502
[26] Lieberman M A and Lichtenberg A J 2005 *Principles of Plasma Discharges and Materials Processing* (New York: Wiley)
[27] Dedrick J *et al* 2017 Phase-resolved optical emission spectroscopy of a neutralizer-free gridded ion thruster *American Institute of Aeronautics and Astronautics: 35th Int. Electric Propulsion Conf. York* (York: The University of York)
[28] Rafalskyi D and Aanesland A 2014 Neutralizer-free gridded ion thruster *50th AIAA/ASME/SAE/ASEE Joint Propulsion Conf.* (Cleveland, OH: AIAA) 3423
[29] Li Y F *et al* 2022 *Plasma Sources Sci. Technol.* **31** 035009
[30] Lafleur T and Rafalskyi D 2018 *Plasma Sources Sci. Technol.* **27** 125004
[31] Roth J R 2001 *Industrial Plasma Engineering: Volume 2: Applications to Nonthermal Plasma Processing* (Boca Raton, FL: CRC Press)
[32] Gahan D *et al* 2012 *Plasma Sources Sci. Technol.* **21** 024004
[33] Gahan D, Dolinaj B and Hopkins M B 2008 *Rev. Sci. Instrum.* **79** 033502
[34] Brihoum M *et al* 2013 *J. Vac. Sci. Technol.* A **31** 020604
[35] Beattie J R and Wilbur P J 1977 *J. Spacecr. Rockets* **14** 747–55
[36] Chabert P and Braithwaite N 2011 *Physics of Radio-Frequency Plasmas* (Cambridge: Cambridge University Press)